NANO LETTERS

pubs.acs.org/NanoLett Letter

Visualizing Quantum Interference in Molecular Junctions

Suman Gunasekaran, Julia E. Greenwald, and Latha Venkataraman*

Cite This: *Nano Lett.* 2020, 20, 2843−2848 Read Online

ACCESS | Metrics & More | Article Recommendations | Supporting Information

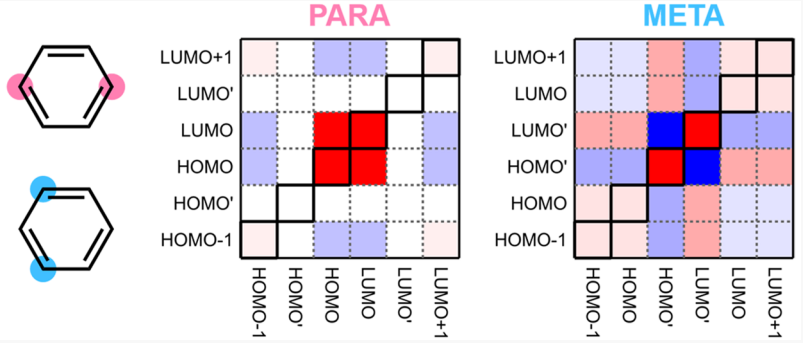

ABSTRACT: Electron transport across a molecular junction is characterized by an energy-dependent transmission function. The transmission function accounts for electrons tunneling through multiple molecular orbitals (MOs) with different phases, which gives rise to quantum interference (QI) effects. Because the transmission function comprises both interfering and noninterfering effects, individual interferences between MOs cannot be deduced from the transmission function directly. Herein, we demonstrate how the transmission function can be deconstructed into its constituent interfering and noninterfering contributions for any model molecular junction. These contributions are arranged in a matrix and displayed pictorially as a QI map, which allows one to easily identify individual QI effects. Importantly, we show that exponential conductance decay with increasing oligomer length is primarily due to an increase in destructive QI. With an ability to "see" QI effects using the QI map, we find that QI is vital to all molecular-scale electron transport.

KEYWORDS: *single-molecule junction, molecular electronics, quantum interference, transmission coefficient, Green's function, Hückel model, conductance decay*

Quantum mechanics dictates electron transport at the nanoscale.[1−4] In single-molecule junctions, where the device size is comparable to the electronic phase coherence length, the phase of the tunneling electron wave influences transport characteristics.[5] Phase differences arise when an electron wave traverses multiple conduction pathways, which introduces quantum interference (QI) effects that may either increase (constructive QI) or decrease (destructive QI) the probability of electron tunneling.[6−11] Pathways can be either atomic orbital-derived spatial paths or molecular orbital (MO)-derived transmission channels. MO-based QI is more generally applicable to molecular junctions and will be the focus of the discussion herein.

The theoretical description of QI between MOs has been well-established.[2,12] An electron incident on a molecular junction may tunnel via multiple MOs. The probability of tunneling via a single level, the ith MO, is described by a Lorentzian transmission function, denoted here as $T_i(E)$

$$T_i(E) = \frac{\gamma_i^2}{(E - \varepsilon_i)^2 + \gamma_i^2} \quad (1)$$

where E is the energy of the incident electron, ε_i is the peak of the Lorentzian and corresponds to the energy of the ith MO, and γ_i denotes the strength of the coupling between the MO and the electrodes.[13,14] An electron wave transmitted through the level experiences a phase shift relative to the incident wave (Figure 1).[15,16] The amplitude and phase of the transmitted wave are described by a complex transmission coefficient t_i, where the transmission probability is the modulus squared of the transmission coefficient[17,18]

$$T_i = |t_i|^2 \quad (2)$$

For a molecular junction, the total transmission probability is the modulus squared of the sum of the complex transmission

Received: February 11, 2020
Revised: March 1, 2020
Published: March 6, 2020

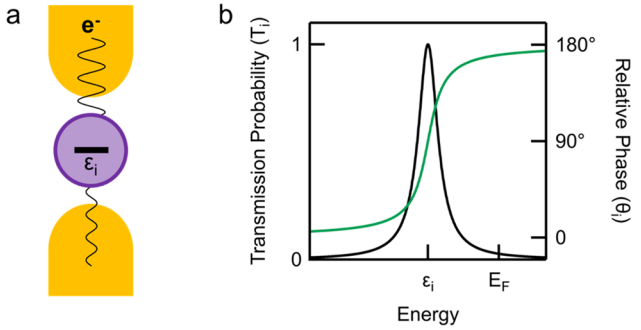

Figure 1. (a) Schematic of molecular junction with a single level, i. The amplitude and phase of the transmitted wave differ from those of the incident wave. (b) Tunneling probability (black) and phase of the transmission coefficient (green) as a function of energy for transport across a single level with energy ε_i.

coefficients for all MOs. For a molecule with two MOs, i and j, the total transmission probability, $T_{i+j}(E)$, is

$$T_{i+j} = |t_i + t_j|^2 = |t_i|^2 + |t_j|^2 + t_i t_j^* + t_i^* t_j \tag{3}$$

The total transmission probability is not merely the sum of the individual transmission probabilities for each MO ($T_{i+j} \neq |t_i|^2 + |t_j|^2$). The cross-terms in eq 3 represent QI between the ith and jth MO, which we denote $T_{ij}(E)$[19]

$$T_{ij} = t_i t_j^* + t_i^* t_j = 2\sqrt{T_i T_j}\cos(\theta_i - \theta_j) \tag{4}$$

where θ_i and θ_j are the complex phases of t_i and t_j, respectively. If θ_i equals θ_j, there is constructive interference between the ith and jth MO, whereas if θ_i and θ_j differ by 180° there is destructive interference. Hence, QI can be understood in terms of phase differences between MO-derived transmission coefficients.[10]

Yoshizawa and co-workers have developed a set of rules to predict the presence of constructive or destructive QI near the Fermi energy for certain simple situations.[20] These rules rely on determining the relative phases of the transmission coefficients of the frontier MOs. Others have developed various pen-and-paper methods for predicting the existence of antiresonances at the Fermi energy.[3,11,21] However, QI is relevant to all molecular junctions, not simply those with transmission functions featuring antiresonances. A general, quantitative technique to easily calculate and visualize QI in all systems is currently lacking. As a result, QI is often overlooked in transmission functions where antiresonances do not appear.

To model electron transport in a molecular junction, the Green's function approach is commonly employed for which the transmission function is calculated as[22]

$$T(E) = \mathrm{Tr}[\Gamma_L G \Gamma_R G^\dagger] \tag{5}$$

where G and $G^\dagger$ are the retarded and advanced Green's functions, and Γ_L and Γ_R are matrices describing the coupling to the left and right electrodes, respectively (see Supporting Information Section 1). The Green's function is typically expressed in the atomic basis.[23] To extract QI between MOs, a change of basis must be performed to transform the Green's function matrix from the atomic basis to the MO basis. This transformation can be achieved using a change of basis matrix, P, whose columns comprise the eigenvectors of G and for which the matrix $P^{-1}GP$ is diagonal. In the MO basis, the transmission function, T, becomes a sum over all MOs, encompassing both the noninterfering, T_i, and interfering terms, T_{ij}[2,24]

$$T = \sum_i T_i + \sum_{i>j} T_{ij} \tag{6}$$

To provide a simple way of calculating the noninterfering and interfering terms, we introduce a matrix, Q, defined as

$$Q(E) = (P^\dagger \Gamma_L G P) \circ (P^{-1}\Gamma_R G^\dagger P^{-1\dagger})^{\mathrm{T}} \tag{7}$$

where $(\circ)$ denotes the entrywise product and $(\bullet)^{\mathrm{T}}$ denotes the matrix transpose. As we show in Supporting Information Sections 2 and 3, the noninterfering transmission probability for the ith MO is simply given by the ith diagonal element of Q

$$T_i = Q_{ii} \tag{8}$$

and the QI between the ith and jth MOs is given by the sum of the (i,j)th and (j,i)th elements of Q

$$T_{ij} = Q_{ij} + Q_{ji} \tag{9}$$

Note that since Q is Hermitian ($Q_{ji}^* = Q_{ij}$), both T_i and T_{ij} are real. Additionally, one can conveniently calculate total transmission excluding interference contributions, denoted here as $\hat{T}$, from the trace of Q

$$\hat{T} = \sum_i T_i = \mathrm{Tr}[Q] \tag{10}$$

The Q matrix therefore deconstructs the transmission function into its constituent interfering and noninterfering components.

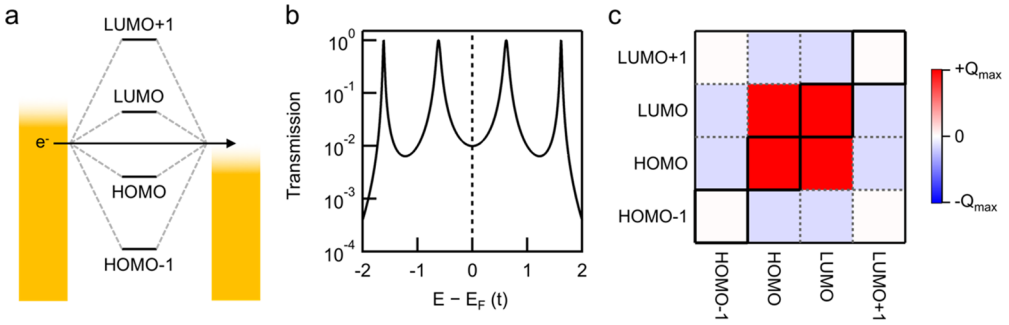

Figure 2. (a) Schematic of MO interference for butadiene. (b) Transmission function for Hückel model of 1−4 butadiene. Energy is expressed in units of t. The dashed line highlights E_F. (c) QI map for 1−4 butadiene at E_F. The main diagonal is highlighted in bold. The off-diagonal squares represent constructive (red) and destructive (blue) QI between MOs. The color scale is normalized to $Q_{max} = \max|Q_{ij}|$.

https://dx.doi.org/10.1021/acs.nanolett.0c00605
Nano Lett. 2020, 20, 2843−2848

Accordingly, a summation of all the elements in Q recovers the total transmission function

$$T = \sum_{ij} Q_{ij} \tag{11}$$

To demonstrate the utility of the Q matrix in elucidating QI effects, we consider a butadiene molecular junction connected to the electrodes at the 1 and 4 positions (i.e., 1−4 butadiene) as an initial example (Figure 2). The π-system of butadiene has four MOs, HOMO−1, HOMO, LUMO, and LUMO+1,which can be modeled at the Hückel level with hopping integral t (see Supporting Information Section 4). Although a tunneling electron "sees" all four MOs as it transits the molecule, which gives rise to QI (Figure 2a),[10] there are no discernible QI effects in the transmission function (Figure 2b). Specifically, the prominence of the four Lorentzian resonance peaks leads one to naïvely believe that the transmission function is merely the sum of the four noninterfering MO-derived resonances. However, calculation of the Q matrix (eq 7) elucidates that QI is in fact important at all energies and between all orbitals.

The Q matrix for 1−4 butadiene at the Fermi energy (E_F) is presented in the form of a heat map (Figure 2c), henceforth referred to as a QI map. Since butadiene has four π-based MOs, the QI map is a 4 × 4 grid. Each square in row i and column j corresponds to the real part of element Q_{ij}. The color of each square represents the sign of the matrix element, with red representing positive values and blue representing negative values. Note that the QI map depicts the Q matrix flipped relative to standard convention (e.g., (1,1) is in the lower left corner). The squares along the main diagonal (highlighted in bold) represent the noninterfering transmission terms (i.e., Q_{ii}) and will necessarily be red. The off-diagonal squares may either be red (constructive QI) or blue (destructive QI). The QI map is always symmetric about the main diagonal since Q is Hermitian. The QI map for 1−4 butadiene shows that in addition to individual contributions from the HOMO and the LUMO, there is constructive interference between the HOMO and LUMO at E_F. Interestingly, the magnitude of the constructive interference between the HOMO and LUMO is comparable to the individual HOMO and LUMO contributions. The HOMO and LUMO also destructively interfere with the HOMO−1 and LUMO+1 (light blue regions in Figure 2c). The full energy-dependent QI map is presented in Video S1. The QI in 1−4 butadiene originates in part from the phase of the MO coefficients at the sites of contact with the electrodes.[20,25] Contacting the molecule at different sites, that is, 1−2, 1−3, and 2−3 butadiene, yields vastly different QI maps (Figure S1).[26]

Comparing meta- and para-benzene further illustrates the connection between QI and MO coefficients. In isolation, benzene possesses doubly degenerate frontier MOs (Figure 3a). When coupled to the electrodes, this degeneracy is lifted, such that the HOMO and HOMO′ and the LUMO and LUMO′ split in energy slightly. Furthermore, the energetic ordering of these MOs depends on the electrical contact sites. For para-benzene, HOMO and LUMO are the frontier MOs, whereas for meta-benzene, HOMO′ and LUMO′ are the frontier MOs. The sites of electrical contact for each molecular junction are highlighted in Figure 3b. The contact sites are explicitly positioned to correspond with the degenerate MOs of the isolated molecule presented in Figure 3a and can be justified by orbital symmetry arguments.[27] The difference in

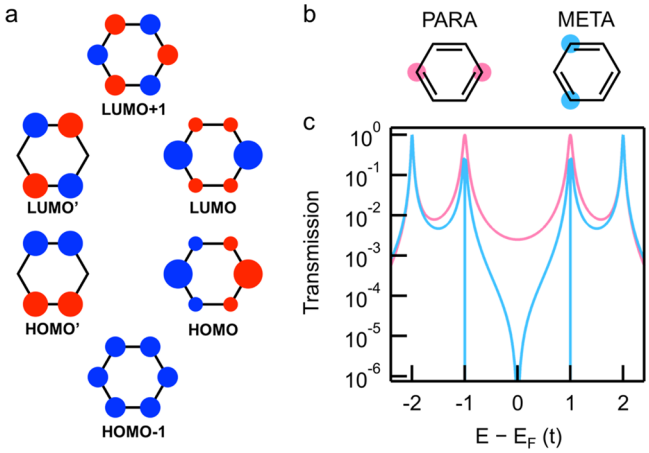

Figure 3. (a) π-based MOs of benzene. (b) Electrical contact sites for molecular junctions of para- and meta-benzene. (c) Transmission functions for para- (pink) and meta-benzene (blue).

contact sites causes meta- and para-benzene molecular junctions to exhibit starkly different transmission functions (Figure 3c).[6,9] Para-benzene exhibits constructive interference at E_F, whereas meta-benzene exhibits complete destructive interference at E_F. At the frontier orbital energies (±1 t in Figure 3c), para-benzene has a resonance feature with unit transmission while meta-benzene has an antiresonance.

The QI maps for para- and meta-benzene illustrate the energy-dependent QI phenomena observed in the transmission functions (Figure 3c). In Figure 4, QI maps for para- and meta-benzene are presented at three different energies: E_F (E = 0 t), the energy of the LUMO resonance (E = +1 t), and an energy between the LUMO and LUMO+1 resonances (E = +1.5 t). In para-benzene, the HOMO and LUMO constructively interfere at E_F (Figure 4a, left). Since the MO coefficients of HOMO′ and LUMO′ are zero at the electrical contact sites (Figure 3a,b), HOMO′ and LUMO′ do not contribute to transmission in para-benzene. This gives rise to the many white squares (i.e., where the Q matrix is zero) in the QI maps, most visible in the QI map at E = 0 t. Although there are no signatures of destructive interference in the transmission function, the blue squares (Figure 4a, left) indicate that the HOMO and LUMO destructively interfere with the HOMO−1 and LUMO+1 akin to 1−4 butadiene (Figure 2c). The QI map for para-benzene at E = +1 t, indicates that transmission is dominated by the LUMO (Figure 4a, center). While other contributions to transmission exist at E = +1 t, they are insignificant compared to the contribution from the LUMO and are not visible with the chosen color scaling.

The QI maps for meta-benzene display strikingly different QI features than those for para-benzene. In meta-benzene, the destructive QI between HOMO′ and LUMO′ at E_F (Figure 4b, left) is equal to the noninterfering contributions of HOMO′ and LUMO′, which gives rise to the antiresonance feature observed in the transmission function (Figure 3c). The QI map at E = +1 t shows strong destructive QI between the LUMO and LUMO′ (Figure 4b, center), which accounts for the sharp spike in the transmission function (Figure 3c). The destructive interference is due to the opposite phases of the MO coefficients for LUMO and LUMO′ at the contact sites. Beyond the LUMO resonance (E = +1.5 t), we observe some interesting changes in color in the QI maps for both para- and meta-benzene. In particular, the interference between the

https://dx.doi.org/10.1021/acs.nanolett.0c00605
Nano Lett. 2020, 20, 2843−2848

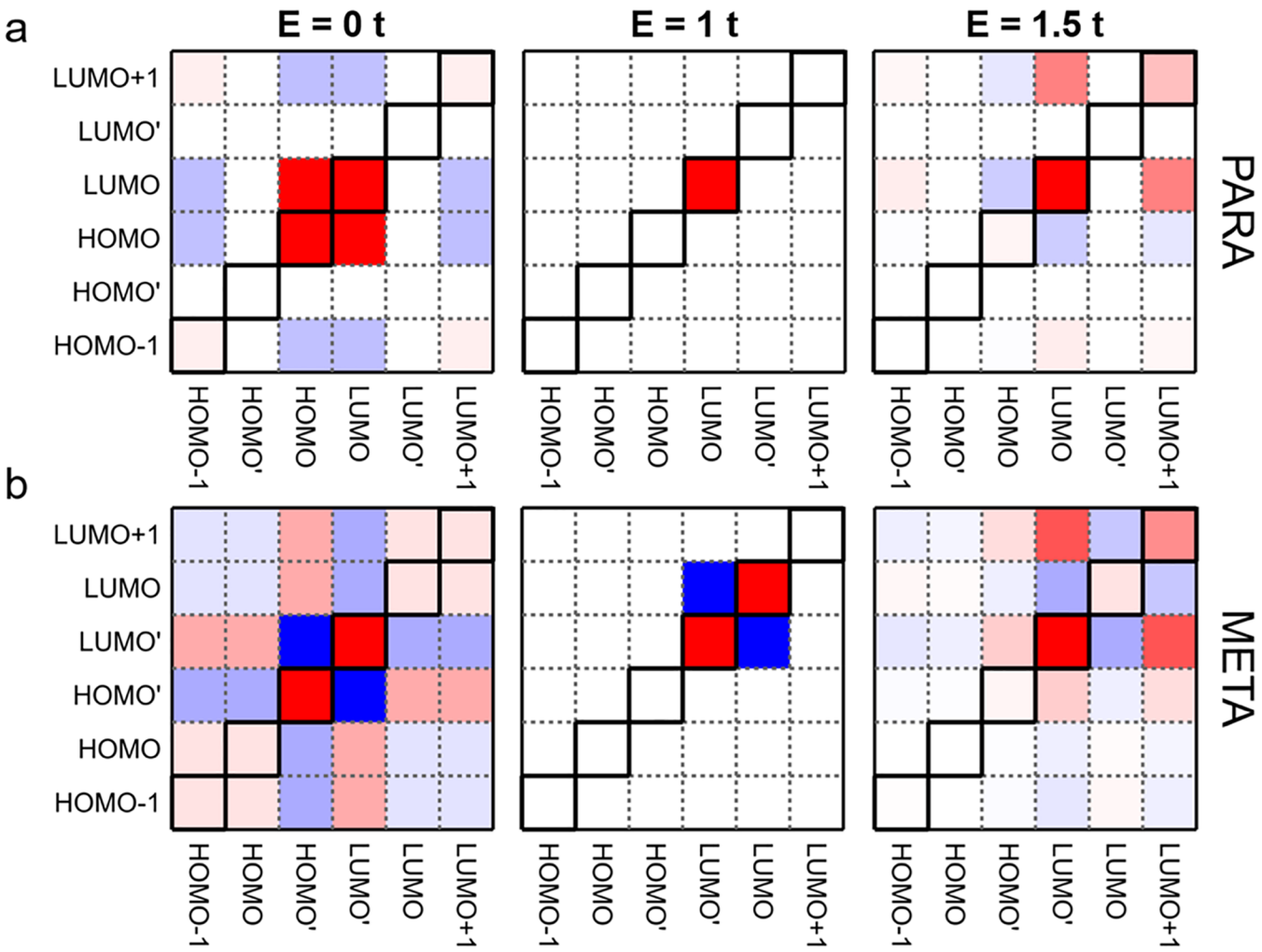

Figure 4. QI maps for (a) para- and (b) meta-benzene at three different energies: 0 t, E_F (left); 1 t, at LUMO resonance (center); and 1.5 t, between LUMO and LUMO+1 (right). Color scale for each QI map is normalized to Q_{max} and therefore is different for each QI map.

frontier MOs changes from constructive to destructive QI for para-benzene (Figure 4a, right) and changes from destructive to constructive QI for meta-benzene (Figure 4b, right). These changes in QI can be attributed to the 180° difference in the phase of the transmission coefficient on either side of a resonance (Figure 1b).[28]

While the above examples are illuminating from a theoretical standpoint, in practice, molecular junctions tend to comprise longer, oligomeric systems. To probe transport properties experimentally, oligomers of varying length are often studied. It has been observed that conductance decays exponentially with oligomer length

$$G \sim e^{-\beta n} \tag{12}$$

where G is the conductance, n is the number of monomer units, and β is the fitting parameter characteristic of the molecular backbone.[29,30] This exponential decay can be reproduced at the Hückel level of theory.[27,31]

To explore the relationship between exponential decay and QI, we model the transmission functions for the oligophenyl series (Figure 5a, n = 1−6). Figure 5b and Figure 5c show the transmission functions for all six oligomers including QI (eq 5) and omitting QI (eq 10), respectively. In both cases, the conductance, approximated as the transmission at E_F, decreases as a function of length (Figure 5d). When QI is included, transmission decays exponentially; however, when QI is omitted, the decay with length is substantially reduced. The modest decrease in conductance observed when QI is omitted can be attributed to a decrease in coupling to the electrodes. As the number of monomer units increases, the MOs become delocalized over longer distances and orbital density throughout the molecular backbone is reduced, which weakens coupling between the MOs and the electrodes. As coupling decreases, the Lorenztian peaks become narrower and transmission at E_F decreases. Previously, decreased coupling has been considered the principle cause of exponential decay with length in molecular junctions.[32] However, direct comparison of conductance with and without QI (Figure 5d) clearly shows that the exponential decay is predominantly due to destructive QI. A similar trend is observed for the polyene series (Figure S2).

We next consider the QI map for n = 6 oligophenyl at E_F (Figure 5e) to understand the origin of the destructive QI. The striking pattern of white squares in the QI map comes from the presence of multiple degenerate uncoupled MOs, which are combinations of HOMO′ and LUMO′ MOs of para-benzene (Figure 4a). The enlarged QI map for the six MOs closest to E_F (Figure 5f) demonstrates that both the noninterfering and interfering transmission contributions from the HOMO−2, HOMO−1, LUMO+1 and LUMO+2 are greater than those

https://dx.doi.org/10.1021/acs.nanolett.0c00605
Nano Lett. 2020, 20, 2843−2848

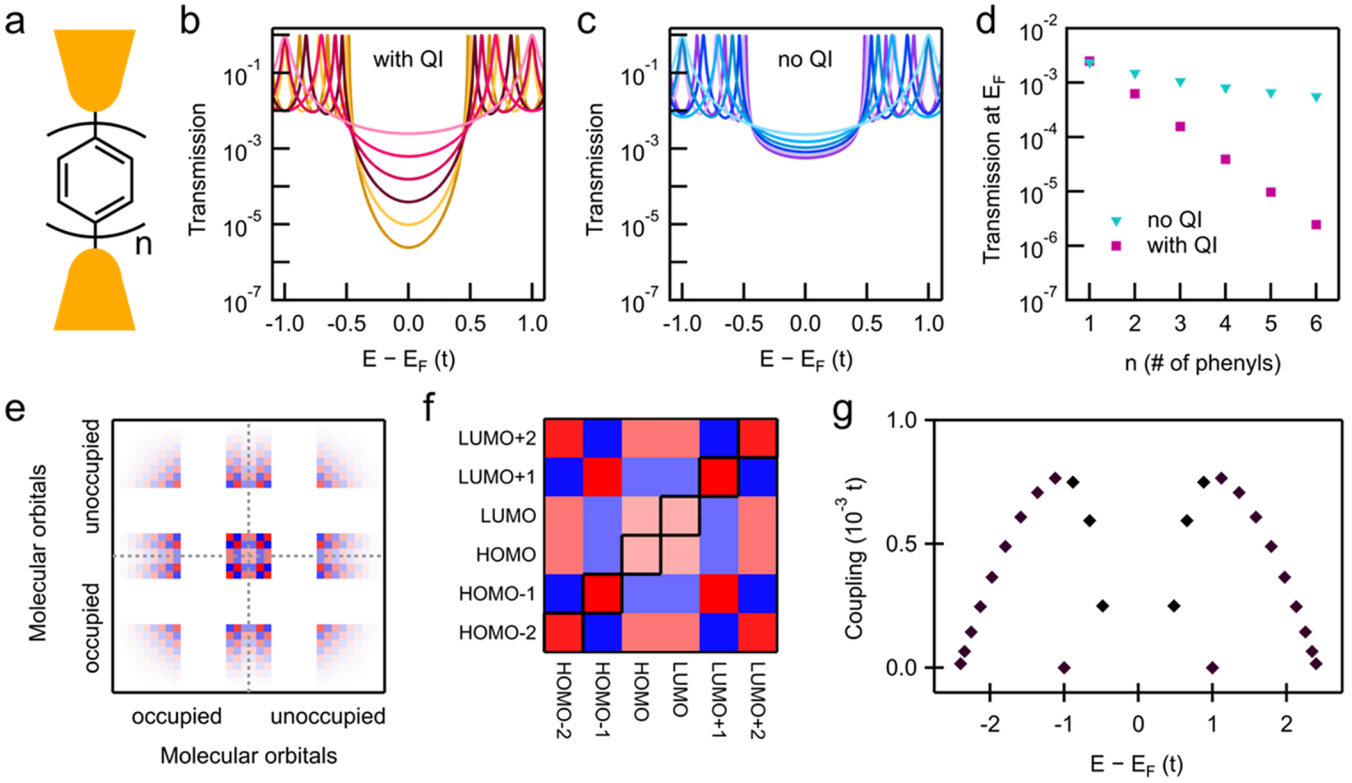

Figure 5. (a) Schematic of oligophenyl molecular junction (n = 1−6). (b,c) Transmission (b) with QI and (c) without QI for oligophenyl series. (d) Transmission at E_F as a function of length for oligophenyl series with QI (magenta) and without QI (turquoise). (e−g) Analysis of n = 6 oligophenyl: (e) QI map at E_F for all 36 π-based MOs, dashed lines placed in between HOMO and LUMO, (f) Enlarged QI map at E_F for the six MOs closest to E_F, (g) MO-electrode coupling vs MO energy for all MOs.

from the HOMO and LUMO. Therefore, even for an oligomer of modest length, the conductance at Fermi is significantly influenced by MOs beyond the frontier MOs. In particular, there exists strong destructive QI between these nonfrontier MOs.

Additional insight can be gleaned from the energy-coupling diagram (Figure 5g) in which MO-electrode coupling versus MO energy is plotted for all 36 π-MOs of n = 6 oligophenyl. This diagram is produced by calculating the real and imaginary parts of the eigenvalues of H+Σ, where H is the Hamiltonian of the molecule and Σ is the self-energy of the electrodes (see Supporting Information Section 1). The degenerate, uncoupled MOs that produce the white squares in the QI map accumulate as single points at $E = \pm 1$ t in the energy-coupling diagram. Importantly, the diagram shows that the HOMO−2, HOMO−1, LUMO+1, and LUMO+2 are better coupled than the HOMO and LUMO and are energetically very close to E_F. This explains why these nonfrontier MOs contribute more significantly to transmission at E_F, as evidenced by the QI map (Figure 5f). The QI maps for n = 1−6 for both the polyene and oligophenyl series (Figures S3 and S4) show that interfering contributions from nonfrontier orbitals increase as a function of oligomer length. Notably, both constructive and destructive QI increase with oligomer length but destructive QI increases more (Figure S5). Therefore, exponential conductance decay with oligomer length can be attributed to an increase in destructive QI from nonfrontier MOs that increasingly influence transport at E_F.

In conclusion, we have shown that quantum interference is ubiquitous in molecular-scale transport. The presence of multiple MOs in a molecular junction means that an incident electron wave may experience interference effects between MOs as it tunnels through the molecular junction. Since QI effects are hard to discern in standard transmission functions, we present a QI map to easily visualize distinct destructive and constructive interference effects between MOs. Using the QI map, we show that exponential decay in conductance as a function of length is due to increasing destructive QI from nonfrontier MOs. Therefore, care must be taken when reducing a molecule to its frontier molecular orbitals and modeling transmission near the Fermi energy using a single Lorentzian or a sum of two Lorentzians. These results highlight that transport in a molecular junction must be viewed holistically, and transmission cannot simply be segregated into contributions from individual, noninterfering MOs.

■ ASSOCIATED CONTENT

Supporting Information

The Supporting Information is available free of charge at https://pubs.acs.org/doi/10.1021/acs.nanolett.0c00605.

Mathematical derivations, model details, and additional figures (PDF)

Energy-dependent QI map for butadiene (MP4)

■ AUTHOR INFORMATION

Corresponding Author

Latha Venkataraman − *Department of Chemistry and Department of Applied Physics and Applied Mathematics, Columbia University, New York, New York 10027, United States;* orcid.org/0000-0002-6957-6089; Email: lv2117@columbia.edu

https://dx.doi.org/10.1021/acs.nanolett.0c00605
Nano Lett. 2020, 20, 2843−2848

Authors

Suman Gunasekaran − *Department of Chemistry, Columbia University, New York, New York 10027, United States;* orcid.org/0000-0001-5974-0642

Julia E. Greenwald − *Department of Chemistry, Columbia University, New York, New York 10027, United States*

Complete contact information is available at: https://pubs.acs.org/10.1021/acs.nanolett.0c00605

Notes

The authors declare no competing financial interest.

■ ACKNOWLEDGMENTS

Valuable discussions with Daniel Hernangómez-Pérez and Ferdinand Evers are gratefully acknowledged. S.G. and J.E.G are supported by NSF Graduate Research Fellowships under Grant DGE-1644869. L.V. acknowledges financial support from the National Science Foundation under award Grant DMR-1807580.

■ REFERENCES

(1) Sun, L.; Diaz-Fernandez, Y. A.; Gschneidtner, T. A.; Westerlund, F.; Lara-Avila, S.; Moth-Poulsen, K. Single-molecule electronics: from chemical design to functional devices. *Chem. Soc. Rev.* **2014**, *43* (21), 7378−7411.

(2) Evers, F.; Korytár, R.; Tewari, S.; van Ruitenbeek, J. M., Advances and challenges in single-molecule electron transport. 2019, *arXiv* https://arxiv.org/abs/1906.10449 (accessed March 5, 2020).

(3) Su, T. A.; Neupane, M.; Steigerwald, M. L.; Venkataraman, L.; Nuckolls, C. Chemical principles of single-molecule electronics. *Nat. Rev. Mater.* **2016**, *1* (3), 16002.

(4) Nitzan, A.; Ratner, M. A. Electron transport in molecular wire junctions. *Science* **2003**, *300* (5624), 1384−1389.

(5) Liang, W. J.; Bockrath, M.; Bozovic, D.; Hafner, J. H.; Tinkham, M.; Park, H. Fabry-Perot interference in a nanotube electron waveguide. *Nature* **2001**, *411* (6838), 665−669.

(6) Sautet, P.; Joachim, C. Electronic interference produced by a benzene embedded in a polyacetylene chain. *Chem. Phys. Lett.* **1988**, *153* (6), 511−516.

(7) Hansen, T.; Solomon, G. C.; Andrews, D. Q.; Ratner, M. A. Interfering pathways in benzene: An analytical treatment. *J. Chem. Phys.* **2009**, *131* (19), 194704.

(8) Solomon, G. C.; Herrmann, C.; Hansen, T.; Mujica, V.; Ratner, M. A. Exploring local currents in molecular junctions. *Nat. Chem.* **2010**, *2* (3), 223−228.

(9) Cardamone, D. M.; Stafford, C. A.; Mazumdar, S. Controlling quantum transport through a single molecule. *Nano Lett.* **2006**, *6* (11), 2422−2426.

(10) Andrews, D. Q.; Solomon, G. C.; Goldsmith, R. H.; Hansen, T.; Wasielewski, M. R.; Van Duyne, R. P.; Ratner, M. A. Quantum Interference: The Structural Dependence of Electron Transmission through Model Systems and Cross-Conjugated Molecules. *J. Phys. Chem. C* **2008**, *112* (43), 16991−16998.

(11) Markussen, T.; Stadler, R.; Thygesen, K. S. The Relation between Structure and Quantum Interference in Single Molecule Junctions. *Nano Lett.* **2010**, *10* (10), 4260−4265.

(12) Solomon, G. C.; Andrews, D. Q.; Hansen, T.; Goldsmith, R. H.; Wasielewski, M. R.; Van Duyne, R. P.; Ratner, M. A. Understanding quantum interference in coherent molecular conduction. *J. Chem. Phys.* **2008**, *129* (5), 054701.

(13) Datta, S. Electrical resistance: an atomistic view. *Nanotechnology* **2004**, *15* (7), S433−S451.

(14) Breit, G.; Wigner, E. Capture of slow neutrons. *Phys. Rev.* **1936**, *49* (7), S19−S31.

(15) Schuster, R.; Buks, E.; Heiblum, M.; Mahalu, D.; Umansky, V.; Shtrikman, H. Phase measurement in a quantum dot via a double-slit interference experiment. *Nature* **1997**, *385* (6615), 417−420.

(16) Yacoby, A.; Heiblum, M.; Mahalu, D.; Shtrikman, H. Coherence and phase sensitive measurements in a quantum dot. *Solid-State Electron.* **1996**, *40* (1−8), 225−231.

(17) Lee, H. W. Generic transmission zeros and in-phase resonances in time-reversal symmetric single channel transport. *Phys. Rev. Lett.* **1999**, *82* (11), 2358−2361.

(18) Taniguchi, T.; Buttiker, M. Friedel phases and phases of transmission amplitudes in quantum scattering systems. *Phys. Rev. B: Condens. Matter Mater. Phys.* **1999**, *60* (19), 13814−13823.

(19) Datta, S.; Melloch, M. R.; Bandyopadhyay, S.; Noren, R.; Vaziri, M.; Miller, M.; Reifenberger, R. Novel Interference Effects between Parallel Quantum Wells. *Phys. Rev. Lett.* **1985**, *55* (21), 2344−2347.

(20) Yoshizawa, K. An Orbital Rule for Electron Transport in Molecules. *Acc. Chem. Res.* **2012**, *45* (9), 1612−1621.

(21) Tsuji, Y.; Hoffmann, R.; Strange, M.; Solomon, G. C. Close relation between quantum interference in molecular conductance and diradical existence. *Proc. Natl. Acad. Sci. U. S. A.* **2016**, *113* (4), E413−E419.

(22) Datta, S. *Electronic transport in mesoscopic systems*; Cambridge University Press: New York, 1995.

(23) Zhao, X.; Geskin, V.; Stadler, R. Destructive quantum interference in electron transport: A reconciliation of the molecular orbital and the atomic orbital perspective. *J. Chem. Phys.* **2017**, *146* (9), 092308.

(24) Solomon, G. C.; Gagliardi, A.; Pecchia, A.; Frauenheim, T.; Di Carlo, A.; Reimers, J. R.; Hush, N. S. Molecular origins of conduction channels observed in shot-noise measurements. *Nano Lett.* **2006**, *6* (11), 2431−2437.

(25) Tsuji, Y.; Yoshizawa, K. Frontier Orbital Perspective for Quantum Interference in Alternant and Nonalternant Hydrocarbons. *J. Phys. Chem. C* **2017**, *121* (17), 9621−9626.

(26) Tsuji, Y.; Hoffmann, R.; Movassagh, R.; Datta, S. Quantum interference in polyenes. *J. Chem. Phys.* **2014**, *141* (22), 224311.

(27) Tada, T.; Yoshizawa, K. Molecular design of electron transport with orbital rule: toward conductance-decay free molecular junctions. *Phys. Chem. Chem. Phys.* **2015**, *17* (48), 32099−32110.

(28) Arroyo, C. R.; Tarkuc, S.; Frisenda, R.; Seldenthuis, J. S.; Woerde, C. H. M.; Eelkema, R.; Grozema, F. C.; van der Zant, H. S. J. Signatures of Quantum Interference Effects on Charge Transport Through a Single Benzene Ring. *Angew. Chem., Int. Ed.* **2013**, *52* (11), 3152−3155.

(29) Choi, S. H.; Kim, B.; Frisbie, C. D. Electrical resistance of long conjugated molecular wires. *Science* **2008**, *320* (5882), 1482−1486.

(30) Kaliginedi, V.; Moreno-Garcia, P.; Valkenier, H.; Hong, W. J.; Garcia-Suarez, V. M.; Buiter, P.; Otten, J. L. H.; Hummelen, J. C.; Lambert, C. J.; Wandlowski, T. Correlations between Molecular Structure and Single-Junction Conductance: A Case Study with Oligo(phenylene-ethynylene)-Type Wires. *J. Am. Chem. Soc.* **2012**, *134* (11), 5262−5275.

(31) Hsu, L. Y.; Rabitz, H. Theory of molecular conductance using a modular approach. *J. Chem. Phys.* **2016**, *145* (23), 234702.

(32) Malen, J. A.; Doak, P.; Baheti, K.; Tilley, T. D.; Segalman, R. A.; Majumdar, A. Identifying the Length Dependence of Orbital Alignment and Contact Coupling in Molecular Heterojunctions. *Nano Lett.* **2009**, *9* (3), 1164−1169.